PROCEEDINGS OF SPIE

SPIEDigitalLibrary.org/conference-proceedings-of-spie

Characterization of a time-resolved spectral detector for spectral fluorescence lifetime imaging with the parallel 16-channel FastFLIM and the phasor analysis

Yuansheng Sun, Trung Duc Nguyen, Yuan-I Chen, Ulas Coskun, Shih-Chu Liao, et al.

Yuansheng Sun, Trung Duc Nguyen, Yuan-I Chen, Ulas C. Coskun, Shih-Chu Liao, Hsin-Chih Yeh, "Characterization of a time-resolved spectral detector for spectral fluorescence lifetime imaging with the parallel 16-channel FastFLIM and the phasor analysis," Proc. SPIE 12384, Multiphoton Microscopy in the Biomedical Sciences XXIII, 1238408 (25 April 2023); doi: 10.1117/12.2656271

SPIE.

Event: SPIE BiOS, 2023, San Francisco, California, United States

Characterization of a time-resolved spectral detector for spectral fluorescence lifetime imaging with the parallel 16-channel FastFLIM and the phasor analysis

Yuansheng Sun[1,*], Trung Duc Nguyen[2], Yuan-I Chen[2], Ulas C. Coskun[1], Shih-chu "Jeff" Liao[1], and Hsin-Chih Yeh[2,3*]

[1] ISS, Inc., 1602 Newton Drive, Champaign, IL 61822, USA.
[2] Biomedical Engineering, The University of Texas at Austin, Austin, TX, USA
[3] Texas Materials Institute, The University of Texas at Austin, Austin, TX, USA

[*] Author to whom correspondence should be addressed:
Yuansheng Sun (Yuansheng.Sun@iss.com); Hsin-Chin Yeh (Tim.Yeh@austin.utexas.edu)

ABSTRACT

Multiplexed fluorescence detection has become an indispensable tool in modern biosensing and imaging. Although a variety of excitation/detection optics designs and unmixing schemes have been proposed to achieve multiplexed detection, successful differentiation and quantification of multiple fluorophores at each imaging pixel is still challenging. Recently, fluorescence lifetime imaging microscopy (FLIM) in combination with the phasor plot analysis has shown many advantages over other multiplexed detection methods. Being an intrinsic property of a fluorescent molecule, fluorescence lifetime measured by FLIM is not biased by excitation power or probe abundance and can reveal information on the probe's microenvironment (ions, pH, oxygen content, electrical signals, index of refractions, etc.). In addition, FLIM is one of the most robust ways of quantifying FRET for studying protein-protein interactions. Moreover, by combining lifetime information with a spectral reading at each pixel, spectral FLIM adds two more dimensions to the spatiotemporal information collected by a conventional confocal setup, resulting in a 6-dimenional (x, y, z, λ, τ, t) data set. The major challenges to the spectral FLIM methods lie in the data acquisition speed and the complexity in post processing and analysis. Here, we present a new time-resolved spectral detector with parallel 16-channel digital frequency domain FLIM (FastFLIM) readouts, for fast spectral FLIM data acquisition. The 16-channel FastFLIM can produce unbiased spectral FLIM data for phasor analysis that unambiguously discriminate and quantitate fluorescent species with unique spectral and lifetime features at each image pixel. Our spectral FastFLIM method offers new opportunities for monitoring multiple dynamic signaling events in live specimens, providing insights into complex biological systems.

1. INTRODUCTION

Fluorescence is one of the many different luminescence processes. The fluorescence processes following light absorption and emission are usually illustrated by the Jablonski diagram [1], and the energy of the emission photon is typically less than that of the absorption photon. Thus, the fluorescence emission of a fluorophore is usually red shifted (longer wavelength) compared to its excitation – a phenomena called the Stokes shift [1]. Measuring fluorescence provides the high degree of specificity amidst non-fluorescing material and the exquisite sensitivity for detecting individual fluorescent molecules. Fluorescence microscopy has been an

Multiphoton Microscopy in the Biomedical Sciences XXIII, edited by Ammasi Periasamy, Peter T. C. So, Karsten König, Proc. of SPIE Vol. 12384, 1238408
 · 1605-7422 · doi: 10.1117/12.2656271

important tool in biological sciences, because it provides excellent sensitivity for quantifying fluorescent molecules in a large dynamic range from high concentrations down to single molecules in live or fixed specimens, over broad spatial and temporal dimensions. Fluorescence microscopy is often employed to image a number of fluorescent probes tagging different sub-cellular components in cells or tissues for studying their colocalization and interactions. This is called multiplexed fluorescence microscopy imaging, which requires precise separation of the fluorescent molecules based on their spectroscopic properties.

It is most common that images of multiple fluorescent probes with different excitation / emission spectral profiles are acquired in different detection channels for multiplexing. The spectral crosstalk between different colored dyes can be minimized by using the dyes with very distinct spectral profiles or completely removed by utilizing some special techniques, such as sequential imaging or spectral linear unmixing. The most advantageous approach for intensity-based multiplexing is spectral imaging microscopy [2-8], which produces λ-stacks consisting of x-, y- (spatial) and λ- (spectral) dimensions, measuring the emission signals in a series of spectral intervals equally sampled over a spectral range, at each pixel location. The emission signals of all spectral windows of the λ-stack can be acquired in parallel by using an array of detectors to dramatically increase the imaging acquisition speed. Linear unmixing of the λ-stack images based on the reference (fingerprint) spectra of pure fluorescent species can be applied to quantitatively separate those components mixed at the same pixel [2-5]. In theory, the number of fluorescent species which can be resolved by spectral imaging and linear unmixing is limited by (no more than) the number of the spectral detection windows [5]. However, the linear unmixing process is computationally challenging and its accuracy and robustness highly depend upon the signal-to-noise (SNR) ratio at each pixel. These limitations could lead to problematic results in many biological applications for using a low excitation dose to minimize phototoxicity at a fast imaging speed (e.g. time-lapse imaging of live specimens). On the other hand, the phasor approach which has been effectively used for processing and analyzing the fluorescence lifetime data [9-16] was applied to the spectral imaging data analysis [6]. It has been demonstrated that the spectral phasor method is an efficient and powerful tool for quantitatively unmixing and analyzing the spectral imaging data and is much faster and more robust for resolving weak hyperspectral signals than the traditional linear unmixing routine [6-8].

Besides the absorption and emission spectra, the fluorophore has other important photophysical properties, such as the extinction coefficient (ability of absorbing photons), the quantum yield (ability of emitting photons) and the fluorescence lifetime – it is the average time the fluorescent molecule spends in the excited state before returning to the ground state. The natural fluorescence lifetime of a fluorophore (in the absence of non-radiative processes) is an intrinsic property of the fluorophore. For most of the fluorescence microscopy methods, the fluorescent signal is quantified by integrating the emitted photons over a period of time which is usually much longer than the fluorescence lifetime - referred to as steady-state (or intensity-based) imaging. In contrast, fluorescence lifetime imaging microscopy (FLIM) measures the fluorescent signal at a very high temporal resolution (down to picoseconds) and is able to resolve the fluorescence lifetime. FLIM provides a totally new dimension to quantitate the fluorescent probe in addition to its steady-state intensity and spectral profiles and opens new opportunities for multiplex imaging. It should be noted that the fluorescence lifetime carries information about the local microenvironment of the fluorescent molecule and can be very sensitive to certain environmental changes. Therefore, with peculiar selectivity of probes, FLIM can provide quantitative information of the probe microenvironment, such as ions, pH, oxygen content, electrical signals, index of refractions, etc [17]. FLIM is widely used to measure Förster resonance energy transfer (FRET) for studying protein-protein interactions [17-19]. It does not require the corrections for spectral bleedthrough that are necessary for intensity-based measurements of sensitized emission from the acceptor. Also, quantifying FRET by FLIM is much less affected by photobleaching and scatter / ambience noise compared to the intensity-based FRET imaging. All these factors make FLIM to be among the most accurate methods of measuring FRET. FLIM has also been employed to investigate a number of human

diseases using endogenous autofluorescent molecules such as FAD, NADH in human cells and tissues and shows great promise in several clinical applications [20-24].

Numerous FLIM methodologies have evolved for various biological and clinical applications [17]. In the last two decades turn-key commercial FLIM systems have become available from several companies including ISS (www.iss.com), making the technique easily accessible. However, FLIM techniques can still be challenging for many biologists because of the complexity in analyzing and interpreting FLIM data. The traditional approach for the determination of the fluorescence decay times consists in using the least-square fitting analysis at each pixel or each group of binned pixels in the image. This approach requires indeed some level of expertise in the choice of the fitting model and a full appreciation of the statistical tools that are to be utilized in cases that are at best disputable. The fitting analysis approach utilized to extract the decay times information significantly hampers the applications of FLIM, when several decay processes are present - it is commonly the case for biological samples. Also, the pixel-by-pixel based fitting process can be time consuming for a large amount of data, although this has been improved by applying new computation algorithms such as machine learning and GPU-based parallelization [25]. To overcome the difficulties in the fitting analysis and simplify the FLIM data analysis, a 2D graphical method for FLIM data presentation and analysis was developed by several research groups, named as polar plot [9], AB plot [10-11], or phasor plot [12-15]. It requires no assumption to be made on the number of decay rates as well as on the specific modeling of the decay. The phasor plot approach leaves all of the fitting problems behind and presents an intuitive simple interface for FLIM users to get instantaneous and quantitative results.

The combination of spectral imaging and FLIM has shown great potentials in quantitative biological and biomedical applications [26-30]. The major challenges to the spectral FLIM method lie in the data acquisition speed and the complexity in post processing and analysis. Recently, it has been demonstrated that the phasor analysis method can significantly simplify the spectral FLIM data presentation and analysis, and yet, produce more accurate and quantitative results for many challenging measurements such as blind unmixing of spectral and lifetime signatures from multiple unknow species and FRET [30]. Here, we present a new time-resolved 16-PMT spectral detector with the true parallel 16-channel digital frequency domain FLIM (FastFLIM) readouts [31,32], for fast spectral FLIM data acquisition and the artifact-free phasor analysis [16]. By combining lifetime information with a spectral reading at each pixel, the spectral FastFLIM technique adds two more dimensions to the spatiotemporal information collected by a conventional confocal setup, resulting in a 6-dimenional (x, y, z, λ, τ, t) data set. It can produce unbiased spectral FLIM data for phasor analysis that unambiguously discriminate and quantitate fluorescent species with unique spectral and lifetime features at each image pixel. Our spectral FastFLIM method offers new opportunities for monitoring multiple dynamic signaling events in live specimens, providing insights into complex biological systems.

2. MATERIALS AND METHODS

2.1 The 16-PMT spectral FastFLIM module

Figure 1 shows the diagram of the 16-PMT spectral FastFLIM module, which includes a grating system, a 16-multianode photomultiplier tube (PMT, model H12310 by Hamamatsu), an overload protection circuit, a RS232C communication circuit, 16 preamplifiers, 16 constant fraction discriminators (CFD) and the 16-channel FastFLIM data acquisition board. The input light beam is coupled to the grating system either in free space or by an optical fiber bundle. The grating disperses the light into the 16 anodes (AN01 to AN16) of the PMT array; the effective area of each anode is 0.8mm × 5mm. The electronic pulse signal (analog) generated from each photon detected by each anode is first pre-amplified and then converted to the LVTTL pulse (digital) by a CFD, which is given to the corresponding input channel of the 16-channel FastFLIM data acquisition board. The 16-channel FastFLIM unit also has the *Pixel*, *Line* and *Frame* scanning clock inputs

for synchronization to a scanning device (e.g. Galvo mirrors), as well as the *clockin* and *clockout* trigger inputs and outputs for synchronization to the laser excitation pulses. For each photon event, the 16-channel FastFLIM unit transfers the time tagged time resolved (TTTR) data to the computer via USB3, containing the information for both micro timing (for the phase / decay histogram) and macro timing (for the correlation), the pixel location and the spectral channel, to build the time resolved emission spectrum (TRES) at each pixel of the image – an example for the illustration is shown in Figure 2.

This 16-anode PMT array features a high quantum efficiency of 45% (at 520 nm) in the visible spectrum (300 nm – 740 nm) and an excellent timing characteristic of less than 300-ps transient spread time (TTS). The gain of each anode can be individually controlled by the computer using the ISS VistaVision software or a simple Python program through the serial communication. This allows shutting off individual PMT channels to avoid the strong laser reflection when the laser excitation wavelengths fall into those spectral windows, making the experimental design more flexible. An overload protection circuit is built in the 16-PMT spectral FastFLIM module to protect the PMT from light overexposure; it monitors the current to each anode and cuts off the power supply to the PMT when the current is over the safety threshold.

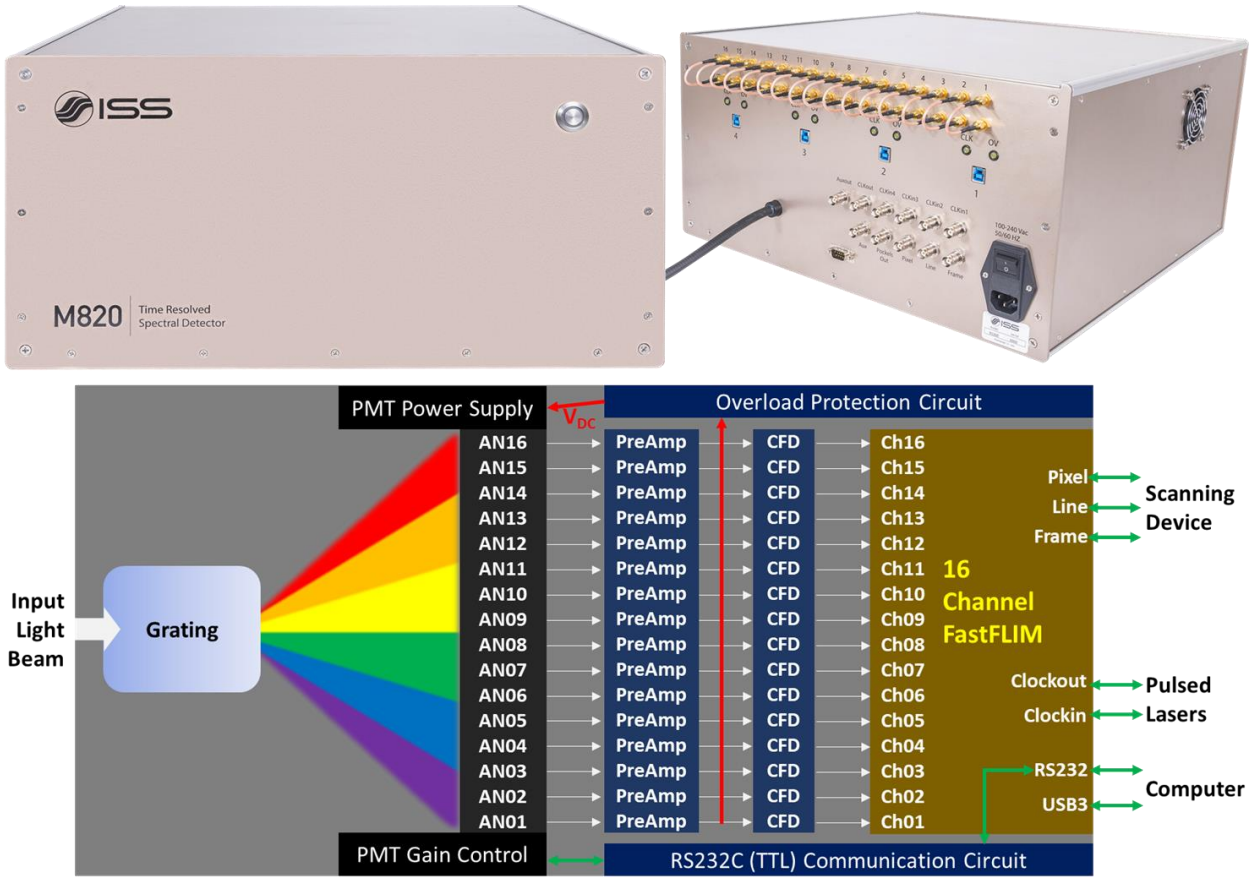

Figure 1: The schematic of the 16-PMT spectral FastFLIM module.

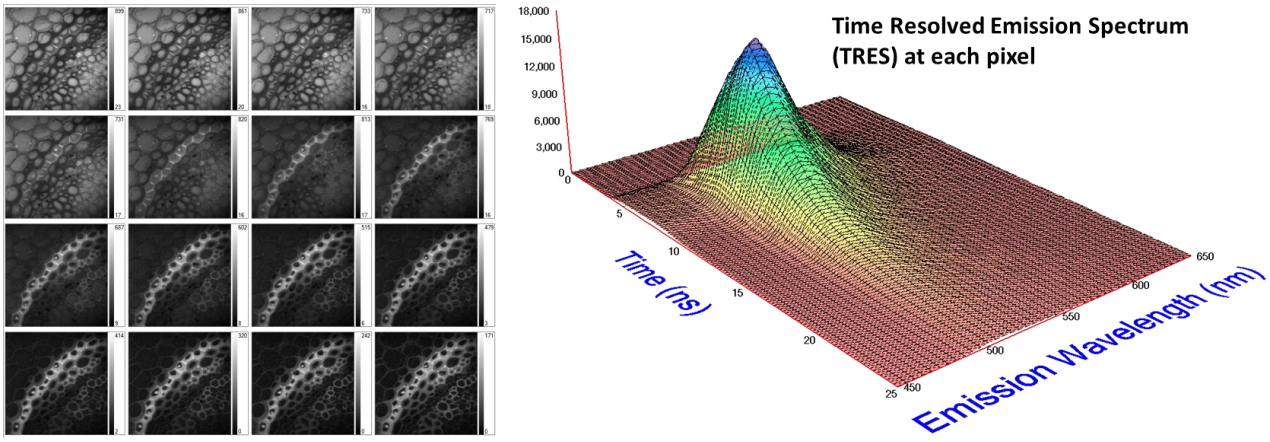

Figure 2: The 16-PMT spectral FastFLIM module produces TRES at each pixel or voxel.

2.2 The instrument setup

In this study, all the spectral FastFLIM experiments were carried out on the ISS Alba *5* laser scanning system attached to a Nikon TiU microscope equipped with the Nikon CFI60 60X / 1.2NA water objective. The 16-PMT spectral FastFLIM data acquisition module was attached to the Alba *5* external port by an optical fiber bundle (Model A12420 by Hamamatsu). The grating system (Model A10766-Y016 by Hamamatsu) has a resolution of 13.4 nm / mm and covers the spectral range of 211.2 nm (from 500.7 nm to 711.9 nm) evenly over the 16 channels. The ISS 405-nm pulsed diode laser driven by the 16-PMT spectral FastFLIM unit (clockout) at the 20MHz repetition rate was used for all the measurements. All the results were obtained by analyzing the 16-PMT spectral FastFLIM data with the ISS VistaVision software.

2.3 The lifetime phasor

For lifetime phasor, each pixel in the spectral FastFLIM data set is transformed to a point ($g\tau$, $s\tau$), called lifetime phasor, on the lifetime phasor plots, based on Eq. (1).

$$g\tau_{x,y,s}(\omega) = m_{x,y,s}(\omega) \cdot \cos[\varphi_{x,y,s}(\omega)]\ ,\ \ s\tau_{x,y,s}(\omega) = m_{x,y,s}(\omega) \cdot \sin[\varphi_{x,y,s}(\omega)] \qquad \text{Eq. (1)}$$

where $m_{x,y,s}$ and $\varphi_{x,y,s}$ are the modulation ratio (m) and the phase delay (φ) measured at a particular modulation frequency (ω) for the (x,y) pixel location in the s-th spectral window of the spectral FastFLIM data set. This transformation can be applied to the time-domain (TD) lifetime image through the digital Fourier transform (DFT), given by Eq. (2).

$$g\tau_{x,y,s}(\omega) = \frac{\int_0^\infty I_{x,y,s}(t)\cdot\cos(\omega t)dt}{\int_0^\infty I_{x,y,s}(t)dt}\ ,\ \ s\tau_{x,y,s}(\omega) = \frac{\int_0^\infty I_{x,y,s}(t)\cdot\sin(\omega t)dt}{\int_0^\infty I_{x,y,s}(t)dt},\ \ \omega = n\cdot 2\pi f \qquad \text{Eq. (2)}$$

where $I_{x,y,s}(t)$ is the number of the photon counts recorded for each time bin "t" at the (x,y) pixel location in the s-th spectral window of the spectral TD-FLIM data set; ω is the angular frequency; f is the repetition frequency of the pulsed excitation light and n is the integer starting from 1.

Although in theory the phasor plot approach can be equally applied to both the FD/DFD and the TD FLIM data, in practice more attentions are required for transforming the TD decay data into the phasor space in order to avoid the erroneous results. The transformation requires one entire period of the decay to be available in the time record, which cannot be achieved by the default settings in most of time correlated single

photon counting (TCSPC) measurements; this can cause artifacts for the phasor plot analysis especially when the excitation repetition time is not long enough to allow the complete decay [16]. In contrast, the DFD FLIM (also known as FastFLIM) technique acquires the data in equal phase cycles in almost 100% duty cycle, perfectly designed for the DFT process, providing distortion-free data for the phasor plot processing and analysis [16]. The data acquired by FastFLIM can be instantly shown on the phasor plots on the fly of data acquisition, providing a live feedback for investigating the change in lifetimes.

The relationships between the phasor and the lifetime are given by Eq. [3], where N is the number of the fluorescent species, and f_i is the fractional contribution of the i-th species of the fluorescence lifetime τ_i to the total intensity. For a single-lifetime species (N = 1), Eq. [3] is reduced to Eq. [4] and the lifetime can be directly determined by the coordinate values of a phasor. It is further derived that the two coordinates of a phasor representing a single-lifetime species must have the relationship defined by "$(g - 0.5)^2 + s^2 = 0.25$", which is drawn as a semicircle curve centering at (g = 0.5, s = 0) with a radius of 0.5 on the phasor plots.

$$g\tau(\omega) = \sum_{i=1}^{N} \frac{f_i}{1+\omega^2\tau_i^2}\,,\ s\tau(\omega) = \sum_{i=1}^{N} \frac{\omega f_i \tau_i}{1+\omega^2\tau_i^2} \qquad \text{Eq. (3)}$$

$$g\tau(\omega) = \frac{1}{1+\omega^2\tau^2}\ ,\ s\tau(\omega) = \frac{\omega\tau}{1+\omega^2\tau^2}\ ,\ \tau = \frac{s\tau(\omega)}{\omega \cdot g\tau(\omega)} \qquad \text{Eq. (4)}$$

- ***The semicircle is a lifetime ruler on the lifetime phasor plots***. The semicircle (often called the universal semicircle) becomes an explicit lifetime ruler for single-lifetime species on the lifetime phasor plots. It also indicates relative changes in lifetime for complex species such that the lifetimes decrease from left (1, 0) being lifetimes near zero to right (0, 0) being infinite lifetimes (see Figure 3).

- ***The scale of the semicircle ruler is adjustable upon the modulation frequency (ω)***. Given the same single-lifetime value, the lifetime phasor shifts to the left along the semicircle for a lower modulation frequency "ω" which results in an increase of the "s/g" ratio (see Eq. [4]). Figure 3 shows an example of comparing the phasor plots of the same lifetime at different modulation frequencies. It also shows the lifetime phasor plots of the 20MHz vs. 80MHz modulation frequencies, demonstrating that the scale of the semicircle ruler can be easily adjusted by selecting the modulation frequency to generate the lifetime phasor plots, making the lifetime phasor plots very flexible to visualize different lifetimes and highlight the contrast upon the lifetime values. It is important to note that a number of modulation frequencies are measured simultaneously by the DFD (FastFLIM) technique.

- ***Single-lifetime species are on the semicircle***. A lifetime phasor population centering at a point on the semicircle indicates a single-lifetime specie.

- ***Complex species are inside the semicircle***. The phasor of a complex species is a linear combination of the individual phasors of single-lifetime species (described below). Connecting these individual phasors on the semicircle yields a convex set inside the semicircle, and thus a species of multiple lifetime components must fall inside the semicircle.

- ***Pixels on the images are mapped to the phasors on the phasor plots, and vice versa***. The pixels with the same lifetime signature fall onto a unique point on the lifetime phasor plots, which coordinate indicates the lifetime information. This feature provides an easy way of visualizing and comparing the lifetime distributions of millions of pixels given by the spectral FLIM data set. On the other hand, selecting a phasor population of a specific lifetime signature on the lifetime phasor plots allows quickly localizing the corresponding pixels to mark or highlight them in the images.

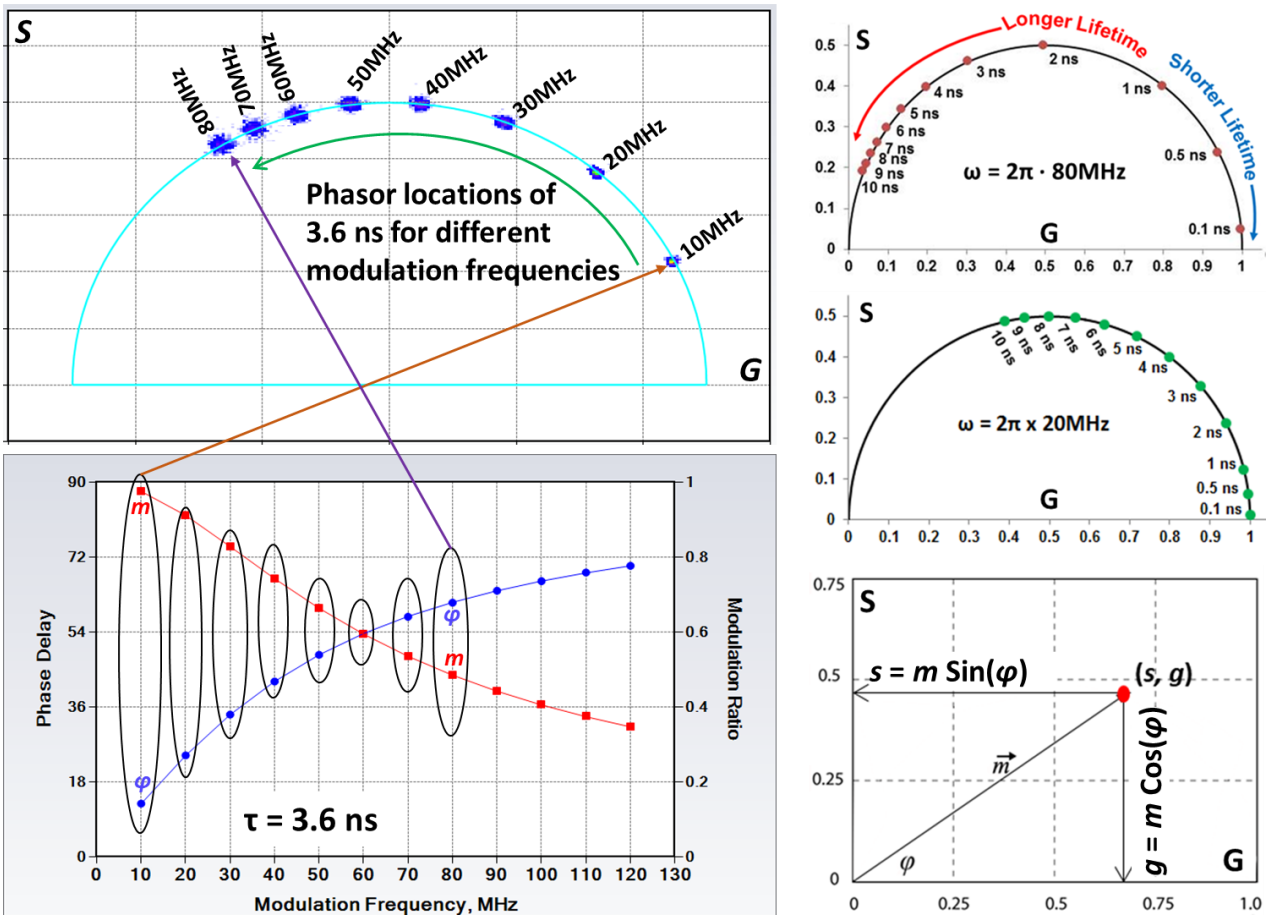

Figure 3: Mapping FastFLIM data to the lifetime phasor plots. The phasor plots can be produced by using a pair of phase (φ) and modulation (m) measured at any modulation frequency (ω), depending upon the lifetime scale to be highlighted. For any given frequency, the universal semicircle indicates the lifetime changes on the phasor plots such that the lifetimes decrease clockwise along the semicircle.

2.4 The spectral phasor

For spectral phasor, the whole spectrum of each pixel in the 16-PMT spectral FastFLIM data set is transformed to a point ($g\lambda$, $s\lambda$), called spectral phasor, on the spectral phasor plots, based on Eq. (5).

$$g\lambda_{x,y}(\omega) = \frac{\sum_{s=1}^{16}[I_{x,y}(s)\cdot\cos(\omega(s-1))]ds}{\sum_{s=1}^{16} I_{x,y}(s)ds},\ s\lambda_{x,y}(\omega) = \frac{\sum_{s=1}^{16}[I_{x,y}(s)\cdot\sin(\omega(s-1))]ds}{\sum_{s=1}^{16} I_{x,y}(s)ds},\ \omega = \frac{n\cdot 2\pi}{16} \qquad \text{Eq. (5)}$$

where $I_{x,y}(s)$ is the intensity of the s-th spectral window at the (x,y) pixel location of the spectral FastFLIM data set; ω is the angular frequency from zero to 2π and n is the integer starting from 1. In this paper, only the fundamental angular frequency (n = 1) is used for making the spectral phasor plots.

The spectral phasor analysis has many similarities with the lifetime phasor analysis, as both use the Fourier transform to reduce the data (decay or spectrum) into a single point in the phasor space, which is defined by two numbers – the real and imaginary parts of the Fourier transform. Like the lifetime phasor plots, the pixels with the same spectral signature fall onto a unique point on the spectral phasor plots, which

coordinate gives the spectral information. This feature allows interactively mapping between the image pixels and the phasor populations of different spectra given on the spectral phasor plots. On the spectral phasor plots, the wavelengths covered by all the spectral windows having the same spectral width are evenly distributed over 360 degrees. The Fourier transform based on Eq. (5) sets both the starting and the ending wavelengths at the 0- or 360-degree angle and increases the wavelengths in the anticlockwise rotation.

Figure 4 shows the spectral phasor plots of several Gaussian spectra simulated based on the spectral windows given by the combination of the grating system and the 16-PMT array used in this paper. Both the starting (500.7 nm) and the ending (711.9 nm) wavelengths of the entire spectrum are located at the 0- or 360-degree angle. The starting wavelength of a spectral window is shifted by 22.5 (360/16) degrees to that of the previous spectral window in the anticlockwise rotation. As seen from Figure 4, the spectra with different peak wavelengths are clearly separated by the angle (phase) as expected. The phasor given by the wider spectrum in terms of the full width at the half maximum (FWHM) is closer to the center (0,0) location of the spectral phasor plot, such that the amplitude (modulation) of the phasor indicates the width of the spectrum. Thus, the spectral phasor plots can distinguish spectra even with the same emission peak wavelength, as long as their shapes are different. This is shown by comparing the 593.1/60-nm (C), 593.1/95-nm (D) and 593.1/122-nm (E) cases in Figure 4. However, the emission peak shown by the phasor plot can be shifted when the information of the measured spectrum is significantly missing, as shown by the 527.1/100-nm (B) case in Figure 4. This is because the Fourier transform used by the spectral phasor plot works ideally with a periodical function. Typically, this is not a problem for using the signature given by the spectral phasor to identify the corresponding fluorescent species, as long as the same spectral acquisition settings are used.

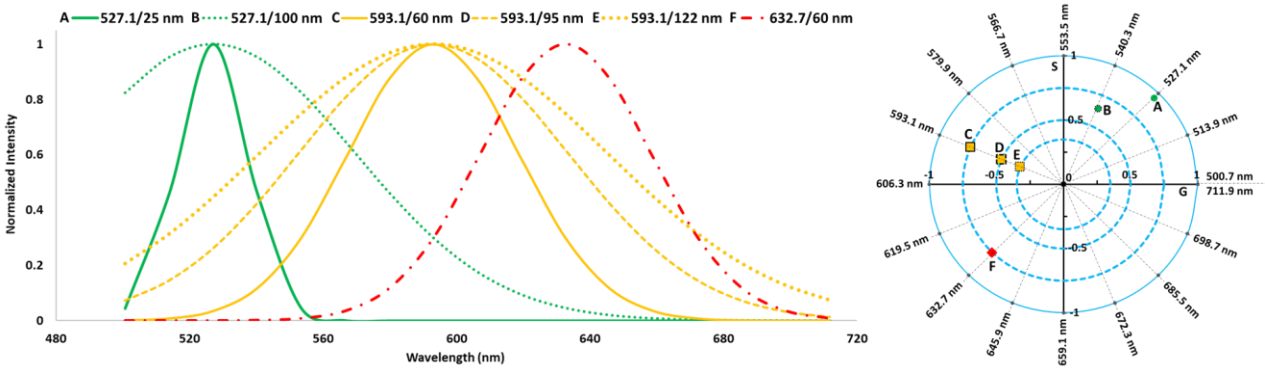

Figure 4: Spectral phasor plots of simulated Gaussian emission spectra centered at the peak wavelengths of 527.1 nm (A, B), 593.1 nm (C, D,E) and 632.7 nm (F) with the FWHM of 25 nm (A), 100 nm (B), 60 nm (C), 95 nm (D), 122 nm (E) and 60 nm (F), respectively.

2.5 The vector rule of the phasor plots

A phasor of a complex species is a linear combination of multiple phasors, each representing an individual species of a pure lifetime or spectrum signature. This is a very important property of the phasor plot for allowing fast vector-based mathematical operations to resolve complex problems. It makes the phasor plot a simple but powerful tool for quantitative spectral FLIM data analysis. Several analysis routines used in the multi-image phasor analysis (MiPA) module of the ISS VistaVision software were developed based on the vector rule of the phasor plots [33]. Figures 5 shows how to unmix two and three lifetime species on the lifetime phasor plots. The same operations can be directly applied to the spectral phasor plot analysis, which routines are now also available in the MiPA module.

- ***The two-species analysis*** routine is illustrated in Figure 5. The phasor coordinate of a mixture composed of two species must lie on the line connecting the two phasors of representing each individual species. In MiPA, two cursors are used to define the phasor coordinates of the two species (S_1 and S_2); for each pixel of the lifetime image(s) mapped to the phasor plots, its phasor point (S) is projected to the line connecting S_1 and S_2 at the intersecting point (S_P) and then unmixed as follows:
  - the fraction of species 1 (f_1) at the pixel is determined by the ratio of the distance between S_2 and S_P over the total distance between S_1 and S_2;
  - the fraction of species 2 (f_2) at the pixel is determined by the ratio of the distance between S_1 and S_P over the total distance between S_1 and S_2.

- ***The three-species analysis*** routine is illustrated in Figure 5. The phasor coordinate of a mixture composed of three species must be inside the triangle formed by the three phasors of representing each individual species. In MiPA, three cursors are used to define the phasor coordinates of the three species (S_1, S_2 and S_3); for each pixel of the lifetime image(s) mapped to the phasor plots, its phasor point (S) is unmixed as follows:
  - the fraction of species 1 (f_1) is determined by the ratio of the triangle area enclosed by connecting S, S_2 and S_3 over the total triangle area by connecting S_1, S_2 and S_3;
  - the fraction of species 2 (f_2) is determined by the ratio of the triangle area enclosed by connecting S, S_1 and S_3 over the total triangle area by connecting S_1, S_2 and S_3;
  - the fraction of species 3 (f_3) is determined by the ratio of the triangle area enclosed by connecting S, S_1 and S_2 over the total triangle area by connecting S_1, S_2 and S_3.

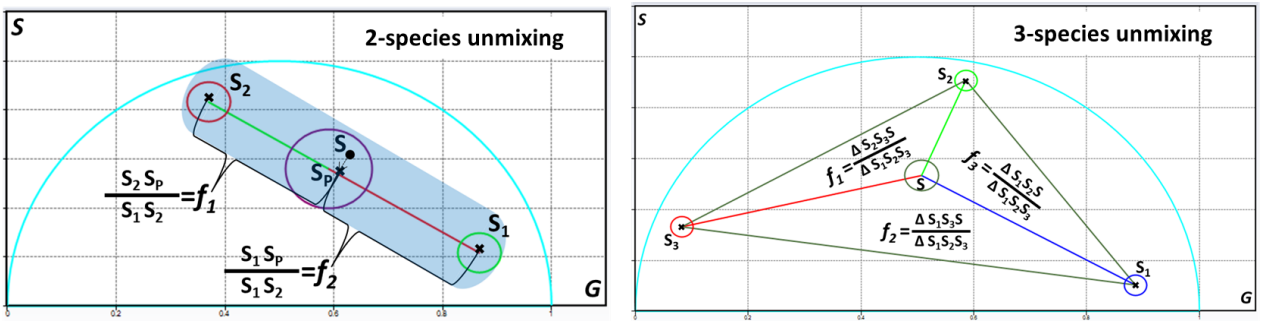

Figure 5: The two-species vs. three-species analysis on the phasor plots.

3. RESULTS AND DISCUSSIONS

3.1 Measurements of the standard fluorescent dyes in solutions

Several standard fluorescent dyes in solutions are measured using the 16-PMT spectral FastFLIM method, including Atto 425 in water, Rhodamine 110 in water, Fluorescein in PBS at pH 7.4, Atto 532 in water, Rose Bengal in water, Rhodamine B in water and Protoporphyrin IX (PPIX) in water. Figure 6 and Figure 7 show their spectral and lifetime phasor plots, respectively. All of them can be clearly differentiated, except that Rhodamine 110 and Fluorescein have nearly identical lifetimes (4 ns). The expected lifetime of each dye is directly obtained from its lifetime phasor plot. On the spectral phasor plots, all the dyes are well separated by

their phase angles (as expected), except for Fluorescein and Rhodamine 110. They are very close in the phase angle due to their similar peak emission wavelengths, but are more (well) separated in the modulation amplitude due to the different shapes of their emission spectra. Figure 6 also shows the comparisons between the emission spectra obtained by the 16-PMT detector and the reference spectra obtained at the 0.1-nm spectral resolution (https://searchlight.semrock.com/), for three example dyes (Rhodamine 110, Atto 532 and PPIX). Despite the obvious deviations due to the very different spectral resolutions and integrations (13.4nm vs. 0.1nm), the spectra measured by the 16-PMT detector follow the reference spectra well.

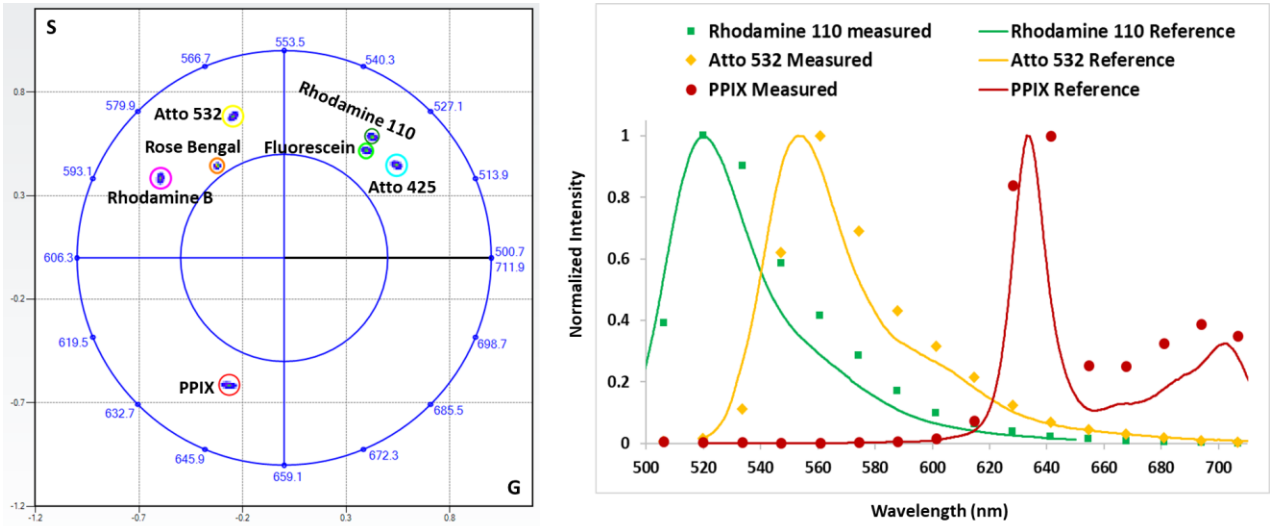

Figure 6: The spectral phasor plots of several individual fluorescent dyes in solutions.

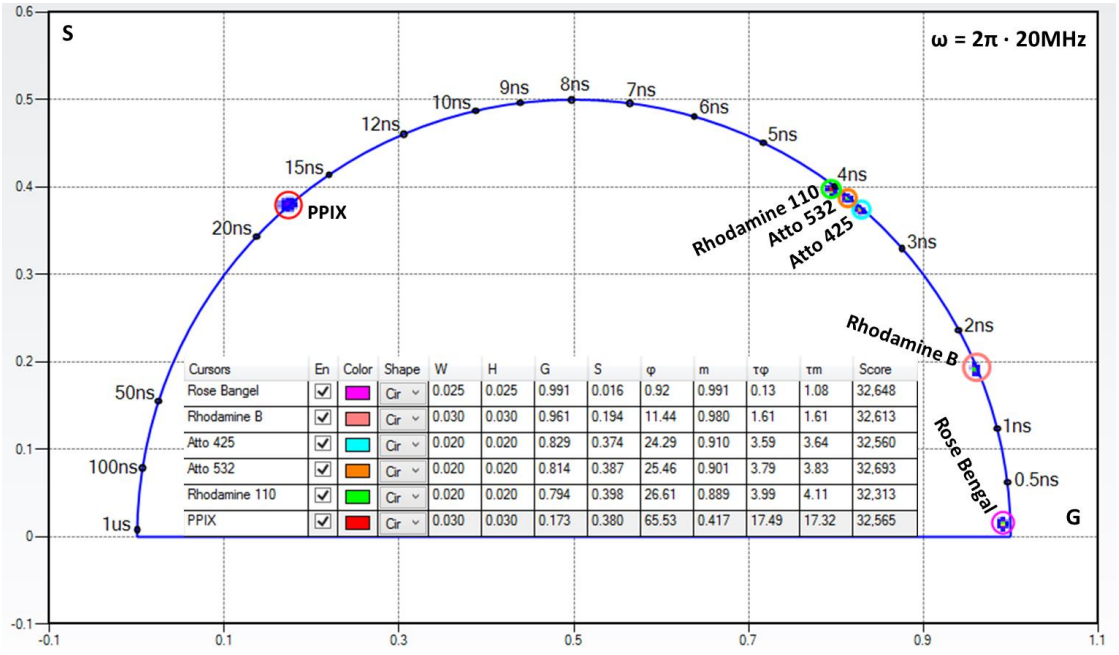

Figure 7: The lifetime phasor plots of several individual fluorescent dyes in solutions.

Using the 3-species unmixing analysis in MiPA (see Section 2.5 and Figure 5), the mixture of three fluorescent dyes of different lifetimes can be decomposed to obtain the fraction (intensity) contribution of each individual species. A measurement example of using three fluorescent dyes (Rhodamine 110, Acridine Orange and Rose Bengal) in water was demonstrated earlier [33] and shown in Figure 8 (left). The measurements of three individual dyes and the mixtures of each pair and all three dyes (totally seven data sets) are given on the lifetime phasor plots. As expected, the phasor population of the mixture of two dyes lies on the line of connecting those of the two individual dyes, and the phasor population of the mixture of three dyes lies inside the triangle enclosed by those of the three individual dyes. Applying the three-species unmixing analysis, the intensity contributions of Rhodamine 110 (38.5%), Acridine Orange (38.6) and Rose Bengal (22.9%) to the mixture are obtained.

The same 2-species unmixing routine in MiPA can be directly applied the spectral phasor plots to quantitatively separate three fluorescent dyes of different emission spectrum. Figure 8 (right) also shows a measurement example of unmixing three fluorescent dyes (Atto 425, Fluorescein and Rhodamine B) in water on the spectral phasor plots. The measurements of three individual dyes and their mixture are given on the spectral phasor plots, and the phasor population of the mixture lies inside the triangle enclosed by those of the three individual dyes. Applying the three-species unmixing analysis, the intensity contributions of Atto 425 (45.8%), Fluorescein (16.9) and Rhodamine B (37.3%) to the mixture are obtained.

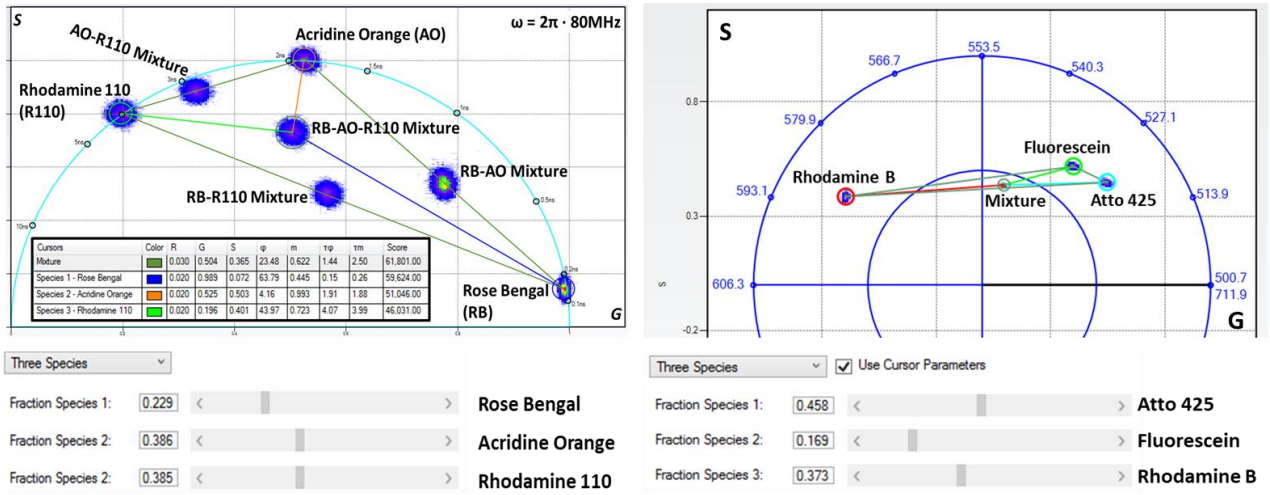

Figure 8: The 3-species spectral vs. lifetime phasor unmixing of the mixtures of three fluorescent dyes.

Both the 2-species and the 3-species unmixing analysis routines in MiPA (described in Section 2.5) can be directly applied to the lifetime and spectral phasor plots of the 16-PMT spectral FastFLIM data, to quantitatively separate a number of fluorescent species based on their lifetime and spectral signatures at each pixel. These processes are instant since the mathematical (vector-based) operations are very simple. More importantly, all the pixels of the same lifetime / spectral signature in the image are combined at the phasor location; this global binning by the phasor analysis provides a high SNR, yet without any artifact. The phasor analysis is truly unbiased and an ideal global analysis method for processing and analyzing the complex data given the spectral FastFLIM method. Three examples of using the biological samples are shown below to demonstrate the powerful combination of the 16-PMT spectral FastFLIM technique and the phasor analysis.

3.2 Measurements of the pollen grains sample

Figure 9 shows the measurements and processed results of the pollen grains sample using the 16-PMT spectral FastFLIM technique and the spectral phasor plots analysis. The composite image is produced by summing all the TRES photons at each pixel. There are four phasor populations on the spectral phasor plots, each representing a unique spectral signature. Four coloured (green, yellow, orange and red) cursors covering different phasor populations are used to mark the corresponding pixels of the same phasor population (spectral signature). As shown by the image highlighted by phasors, the three pollen grains of different colors (yellow, orange and red) and the background (green) are clearly identified. It should be noted that for better visualization the false color selected for presenting each spectral signature is not the same as its true color. Using the 2-species spectral phasor unmixing routine, the intensity at each pixel of the composite image is decomposed into two components corresponding to the pollen grain spectrum represented by the yellow or orange or red phasor vs. the background spectrum represented by the green phasor. This process produced three background-free unmixed images pseudo-colored by yellow, orange and red. Merging them yielded the unmixed overlay image for visualizing and comparing different colored pollen grains in the same picture.

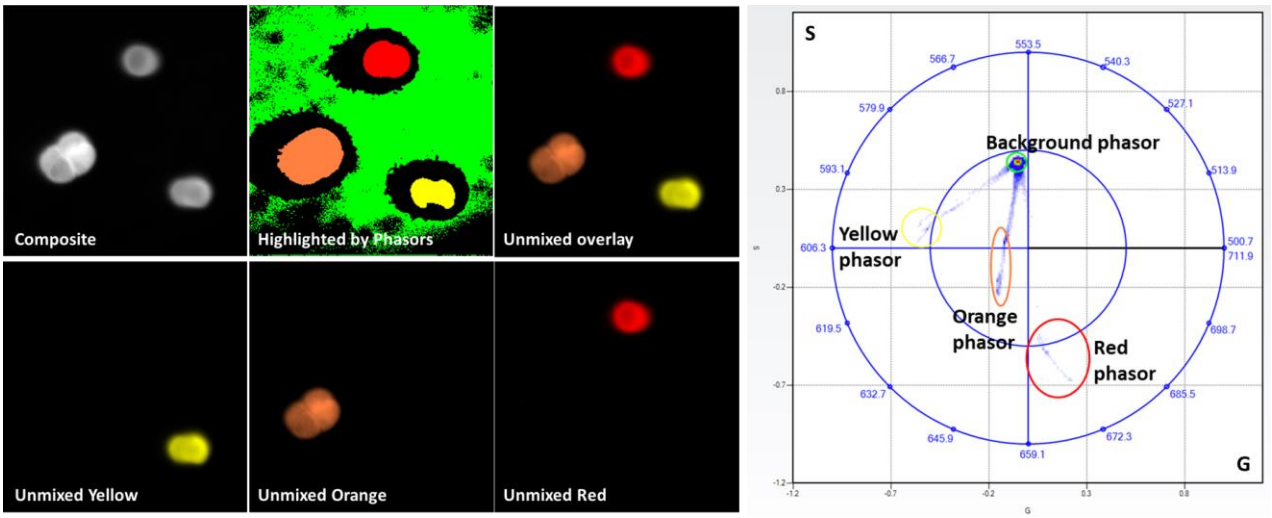

Figure 9: The spectral phasor unmixing and background removal of the pollen grains sample.

3.3 Measurements of the FluoCell™ sample

Figure 10 shows the measurements and processed results of the FluoCell™ slide #1 sample (www.thermofisher.com/order/catalog/product/F36924) using the 16-PMT spectral FastFLIM technique and both the spectral and lifetime phasor plots analysis. This BPAE cellular sample has three fluorescent labels – DAPI for nucleus, MitoTracker™ Red (MTR) for mitochondria and Alexa Fluor™ 488 (AF488) for phalloidin. The composite image is produced by summing all the TRES photons at each pixel. On the spectral phasor plots, the phasors of the background vs. the fluorescent signals are clearly separated, and using a cursor covering the background phasor identifies the background pixels on the composite image - this phasor information is used to remove the background. The unmixed MTR image of the red pseudo color is obtained using the 3-species spectral phasor unmixing routine. However, the DAPI and the AF488 spectral phasors are very close, because a significant part of the DAPI emission spectrum (< 500.7 nm) is missing and its spectral phasor is shifted. Thanks to the time-resolved (lifetime) information also provided by the spectral FastFLIM technique, the AF488 phasor is well separated from the DAPI and MTR phasors on the lifetime phasor plots. This makes an easy separation of the AF488 signal from the DAPI and MTR signals, producing the unmixed AF488 image of the green pseudo color. The DAPI signal is teased out by the 2-specis lifetime phasor

unmixing between the DAPI and the MTR phasors, to generate the unmixed DAPI image of the cyan pseudo color. Finally, the three unmixed images are overlaid to produce the unmixed overlay image for visualizing how the three fluorescent tags are distributed in the same cell.

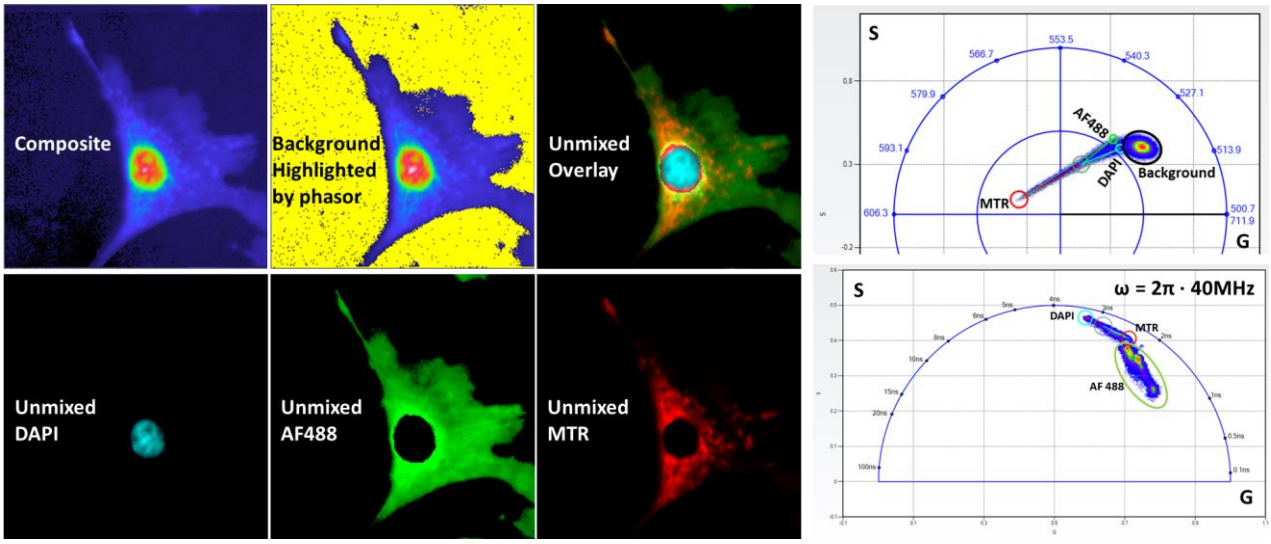

Figure 10: The spectral and lifetime phasor unmixing and background removal of the FluoCell™ sample.

Since only a single excitation wavelength of 405 nm is used in this experiment and it is far away from the peak absorption wavelengths of the AF488 and MTR fluorophores, the emission signals of the AF488 and the MTR are much weaker than that of the DAPI, making a challenging case for quantitative unmixing. On the other hand, it should be pointed out that the 16-PMT spectral FastFLIM technique is totally compatible with multiple excitation wavelengths used simultaneously. In fact, the individual gain control for each anode of the 16-PMT array makes using multiple excitation wavelengths easier and more flexible. For example, when the excitation wavelength falls into a particular spectral window, the gain of the corresponding PMT anode can be set to zero to avoid the saturation due to the strong laser scatters. Also, given the time resolved capability, the 16-PMT spectral FastFLIM technique can be combined with using the pulsed interleave excitation (PIE) wavelengths to greatly extend its utilities [34-36].

3.4 Measurements of the *Convallaria* sample

Figure 11 shows the measurements and processed results of the *Convallaria* sample using the 16-PMT spectral FastFLIM technique and both the spectral and lifetime phasor plots analysis. The composite image is produced by summing all the TRES photons at each pixel. Both the spectral and the lifetime phasor plots indicate that there are two fluorescent species mixed in the sample. The 2-species spectral phasor unmixing separates the two components of the shorter (pseudo-colored by green) and the longer (pseudo-colored by red) wavelengths – overlaying them further produces the spectrally unmixed overlay image. On the other hand, the 2-species lifetime phasor unmixing is applied to the spectral FastFLIM data acquired in the spectral window of 540.3 - 553.5 nm, and separates the two components of the longer (pseudo-colored by green) and the shorter (pseudo-colored by red) lifetimes – overlaying them generates the lifetime-unmixed overlay image. As expected, the distributions of the two fluorescent species shown in the spectrally unmixed overlay image vs. the lifetime-unmixed overlay image are almost the same, such that the species of the shorter and the longer wavelengths have the longer and the shorter fluorescence lifetimes, respectively. However, subtle differences between them are also observed - as pointed out by the white arrows in both unmixed overlay

images, the bright small dots appear purely green in the spectrally unmixed overlay image but more red in the lifetime-unmixed overlay image, indicating that the fluorescent species of the shorter wavelength located in these bright small dots have much shorter lifetimes than most of the same species located in the other places. This is not surprising because the fluorescent lifetime of a fluorescent molecule can vary significantly upon its microenvironment, as described above in the introduction. This example demonstrates that the 16-PMT spectral FastFLIM technology in combination of the phasor analysis can not only differentiate different fluorescent species in the same pixel but also localize the changes of their photophysical properties.

Fluorescence lifetime can be a quantitative tool to monitor many biological processes (such as ion concentration, pH, oxygen content, etc.) in live cells and tissues. FLIM is also one of the most robust methods to measure FRET efficiency for studying protein-protein interactions and tracking dynamic signaling events in live cells [17-19]. With the capability to resolve lifetime and emission spectrum at each pixel, we envision the 16-PMT spectral FastFLIM to soon become a widely adopted technique by researchers to investigate fundamental biological processes in live samples.

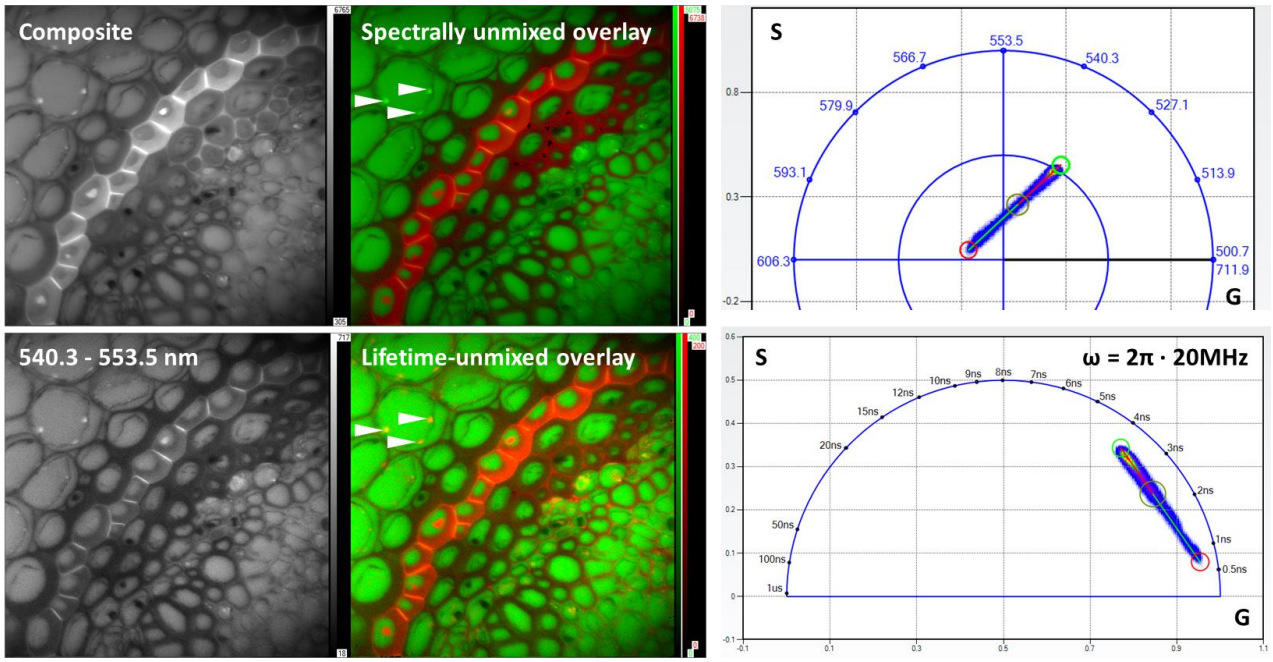

Figure 11: The spectral vs. lifetime phasor unmixing of the *convallaria* sample.

4. CONCLUSION

The spectral FastFLIM technique described in this report combines both temporally and spectrally resolved imaging schemes in creating a true parallel data acquisition mode. It not only acquires the TRES data at each pixel or voxel but also provides rich information in up to six dimensions (x, y, z – spatial coordinates; λ – emission spectra, τ – fluorescence lifetimes; t – time lapse). Besides, analyzing the rich and complex data produced by the spectral FastFLIM can be facilitated by the phasor plot approach. In particular, the spectral FastFLIM produces unbiased spectral FLIM data for distortion-free phasor analysis that can unambiguously discriminate and quantitate fluorescent species with unique spectral and lifetime features at each image pixel.

We demonstrate the integration of spectral FastFLIM with phasor analysis can create a powerful tool for multiplexed imaging. This tool can be an enabling technique to investigate many processes in the life science, including probing protein-protein interactions and dynamic signaling events by FRET, and tracking metabolic changes in complex environments by autofluorescence imaging.

ACKNOWLEDGEMENTS

We are indebted to Dr. Enrico Gratton at LFD, University of California-Irvine for his original developments of the Digital Frequency Domain (DFD) technology and the phasor analysis methods for both fluorescence lifetime and spectral data. The support for H.-C.Y. was from the National Institutes of Health (EY033106) and the National Science Foundation (2235455).

REFERENCES

[1]. J.R. Lakowicz, "Principles of fluorescence spectroscopy," *Springer*, New York (2006).
[2]. M.E. Dickinson, G. Bearman, S. Tille, R. Lansford and S.E. Fraser, "Multi-spectral imaging and linear unmixing add a whole new dimension to laser scanning fluorescence microscopy," *BioTechniques* 31, 1272-1278 (2001).
[3]. T. Zimmermann, J. Rietdorf, A. Girod, V. Georget and R. Pepperkok, "Spectral imaging and linear un-mixing enables improved FRET efficiency with a novel GFP2–YFP FRET pair," *FEBS Letters* 531, 245-249 (2002).
[4]. T. Zimmermann, J. Rietdorf and R. Pepperkok, "Spectral imaging and its applications in live cell microscopy," *FEBS Letters 546*, 87-92 (2003).
[5]. T. Zimmermann, "Spectral imaging and linear unmixing in light microscopy," *Adv Biochem Eng Biotechnol*. 95, 245-265 (2005).
[6]. F. Fereidouni, A.N. Bader and H.C. Gerritsen, "Spectral phasor analysis allows rapid and reliable unmixing of fluorescence microscopy spectral images," *Opt. Express* 20, 12729–12741 (2012).
[7]. F. Cutrale, A. Salih and E. Gratton, "Spectral Phasor approach for fingerprinting of photo-activatable fluorescent proteins Dronpa, Kaede and KikGR," *Methods Appl. Fluoresc.* 1(3), 35001 (2013).
[8]. F. Cutrale, V. Trivedi, L.A. Trinh, C.L. Chiu, J.M. Choi, M.S. Artiga and S.E. Fraser, "Hyperspectral phasor analysis enables multiplexed 5D in vivo imaging," *Nat Methods* 14, 149–152 (2017).
[9]. G. I. Redford and R.M. Clegg, "Polar plot representation for frequency-domain analysis of fluorescence lifetimes," *J. Fluoresc.* 15, 805-815 (2005).
[10]. A.H. Clayton, Q.S. Hanley and P.J. Verveer, "Graphical representation and multicomponent analysis of single-frequency fluorescence lifetime imaging microscopy data," *J. Microsc.* 213, 1-5 (2004).
[11]. Q.S. Hanley and A.H. Clayton, "AB-plot assisted determination of fluorophore mixtures in a fluorescence lifetime microscope using spectra or quenchers," J. Microsc. 218, 62-67 (2005).
[12]. M.A. Digman, M. A., V.R. Caiolfa, M. Zamai and E. Gratton, "The phasor approach to fluorescence lifetime imaging analysis," *Biophys. J.* 94, L14-6 (2008).
[13]. C. Stringari, A. Cinquin, O. Cinquin, M.A. Digman, P.J. Donovan and E. Gratton, "Phasor approach to fluorescence lifetime microscopy distinguishes different metabolic states of germ cells in a live tissue," *PNAS* 108, 13582-13587 (2011).
[14]. S. Ranjit, L. Malacrida, D.M. Jameson, E. Gratton, "Fit-free analysis of fluorescence lifetime imaging data using the phasor approach," *Nat. Protoc.* 13(9): 1979-2004 (2018).
[15]. M.A. Digman, V.R. Caiolfa, M. Zamai and E. Gratton, "The phasor approach to fluorescence lifetime imaging analysis," *Biophys. J.* 94, L14-6 (2008).
[16]. S. Ranjit, L. Malacrida and E. Gratton, "Differences between FLIM phasor analyses for data collected with the Becker and Hickl SPC830 card and with the FLIMbox card," *Microsc Res Tech*. 81(9): 980-989 (2018).
[17]. A. Periasamy and R. M. Clegg, "FLIM microscopy in biology and medicine," *CRC Press*, London (2009).
[18]. R.M. Clegg, "Fluorescence resonance energy transfer," In *Fluorescence imaging spectroscopy and microscopy*, X.F. Wang and B. Herman, editors. *John Wiley & Sons Inc.*, New York. 179-251 (1996).
[19]. Y. Sun, R.N. Day and A. Periasamy, "Investigating protein-protein interactions in living cells using fluorescence lifetime imaging microscopy," *Nat. Protoc.* 6, 1324-1340 (2011).
[20]. M.C. Skala, K.M. Riching, A. Gendron-Fitzpatrick, J. Eickhoff, K.W. Eliceiri, J.G. White and N. Ramanujam. "In vivo multiphoton microscopy of NADH and FAD redox states, fluorescence lifetimes, and cellular morphology in precancerous epithelia," *PNAS* 104, 19494-19499 (2007).
[21]. C. Stringari, R.A. Edwards, K.T. Pate, M.L. Waterman, P.J. Donovan and E. Gratton, "Metabolic trajectory of cellular differentiation in small intestine by phasor fluorescence lifetime microscopy of NADH," *Sci Rep.* 2, 568 (2012).

[22]. B.K. Wright, L.M. Andrews, J. Markham, M.R. Jones, C. Stringar, M.A. Digman and E. Gratton, "NADH distribution in live progenitor stem cells by phasor-fluorescence lifetime image microscopy," *Biophys J.* 103(1), L7-L9 (2012).
[23]. K. Torno, B.K. Wright, M.R. Jones, M.A. Digman, E. Gratton and M. Phillips, "Real-time analysis of metabolic activity within lactobacillus acidophilus by phasor fluorescence lifetime imaging microscopy of NADH," *Curr Microbiol.* 66(4), 365-367 (2013).
[24]. T. Hato, S. Winfree, R.N. Day, R.M. Sandoval, B.A. Molitoris, M.C. Yoder, R.C. Wiggins, Y. Zheng, K.W. Dunn, and P.C. Dagher, "Two-Photon Intravital Fluorescence Lifetime Imaging of the Kidney Reveals Cell-Type Specific Metabolic Signatures," *J. Am. Soc. Nephrol.* **28**, 2420-2430 (2017).
[25]. Y. Chen, Y.J. Chang, S.C. Liao, T.D. Nguyen, J. Yang, Y.A. Kuo, S. Hong, Y.L. Liu, H.G. Rylander III, S.R. Santacruz, T.E. Yankeelov and H.C. Yeh, "Generative adversarial network enables rapid and robust fluorescence lifetime image analysis in live cells," *Commun Biol* 5, 18 (2022).
[26]. W. Becker, A. Bergmann, G.L. Biscotti and A. Rueck, "Advanced time-correlated single photopy and imaging in biomedical systems," In *Proc. Commercial and Biomedical Applications of Ultrafast Lasers IV: Lasers and Applications in Science and Engineering Conference*, J. Neev et al. Editors, *SPIE* (2004).
[27]. R. Borlinghaus and L. Kuschel, "Spectral fuorescence lifetime imaging microscopy: new dimensions with Leica TCS SP5," *Nat. Methods* 3, 868 (2006).
[28]. D.M. Owen, E. Auksorius, H.B. Manning, C.B. Talbot, P.A.A. de Beule, C. Dunsby, M.A.A. Neil, and P.M.W. French, "Excitation-resolved hyperspectral fluorescence lifetime imaging using a UV-extended supercontinuum source," *Opt. Lett. 32*, 3408–3410 (2007).
[29]. F. Fereidouni, K. Reitsma and H.C. Gerritsen, "High speed multispectral fuorescence lifetime imaging," *Opt. Express* 21, 11769–11782 (2013).
[30]. L. Scipioni, A. Rossetta, G. Tedeschi and E. Gratton, "Phasor S-FLIM: a new paradigm for fast and robust spectral fluorescence lifetime imaging," *Nat Methods* 18, 542–550 (2021).
[31]. R.A. Colyer, C. Lee and E. Gratton, "A novel fluorescence lifetime imaging system that optimizes photon efficiency," *Microsc. Res. Tech.* 71, 201–213 (2008).
[32]. Y. Sun, U. Coskun, S.-C. J. Liao and B. Barbieri, "FastFLIM, the all-in-one engine for measuring photoluminescence lifetime of 100 picoseconds to 100 milliseconds," *Proc. SPIE 10498, Multiphoton Microscopy in the Biomedical Sciences XVIII*, 104980W (2018).
[33]. Y. Sun, U.C. Coskun, S.C. Liao and B. Barbieri, "Quantitative tools in the Multi-image Phasor Analysis (MiPA)," *Proc. SPIE 11965, Multiphoton Microscopy in the Biomedical Sciences XXII*, 119650A (2022).
[34]. J. Hendrix and D.C. Lamb, "Pulsed interleaved excitation: principles and applications," *Biophys. J.* 105:848-861 (2013).
[35]. Y. Sun, U. Coskun, A.C. Ferreon, B. Barbieri and S.C. Liao, "Tunable PIE and synchronized gating detections by FastFLIM for quantitative microscopy measurements of fast dynamics of single molecules," *Proc. SPIE 9712, Multiphoton Microscopy in the Biomedical Sciences XVI*, 97120S (2016).
[36]. C.A. Reissaus, K.H. Day, R.G. Mirmira, K.W. Dunn, F.M. Pavalko and R.N. Day, "PIE-FLIM Measurements of Two Different FRET-Based Biosensor Activities in the Same Living Cells," *Biophys. J.* 118(8):1820-1829 (2020).